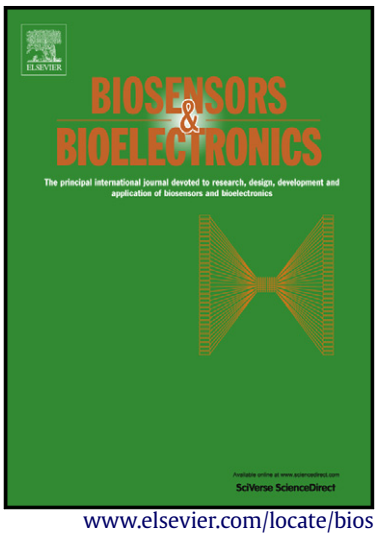


www.elsevier.com/locate/bios

# Biosensing enhancement using passive mixing structures for microarray-based sensors

N. Scott Lynn Jr., José-Israel Martínez-López, Markéta Bocková, Pavel Adam, Victor Coello, Héctor R. Siller, Jiří Homola

PII: S0956-5663(13)00805-1
DOI: http://dx.doi.org/10.1016/j.bios.2013.11.027
Reference: BIOS6363

To appear in: *Biosensors and Bioelectronics*

Received date: 13 September 2013
Revised date: 17 October 2013
Accepted date: 6 November 2013

Cite this article as: N. Scott Lynn Jr., José-Israel Martínez-López, Markéta Bocková, Pavel Adam, Victor Coello, Héctor R. Siller, Jiří Homola, Biosensing enhancement using passive mixing structures for microarray-based sensors, *Biosensors and Bioelectronics,* http://dx.doi.org/10.1016/j.bios.2013.11.027

# Biosensing enhancement using passive mixing structures for microarray-based sensors

N. Scott Lynn Jr.[1], José-Israel Martínez-López[2], Markéta Bocková[1], Pavel Adam[1], Victor Coello[3], Héctor R. Siller[2], Jiří Homola[1*]

[1] Institute of Photonics and Electronics, Chaberská 57, 18251 Prague, Czech Republic; homola@ufe.cz

[2] Tecnológico de Monterrey, Eugenio Garza Sada 2501 Sur, C.P. 64849 Monterrey, N.L., México; israel@null.net, hector.siller@itesm.mx

[3] Centro de Investigación Científica y de Educación Superior de Ensenada, Unidad Monterrey, Alianza Sur No. 105, Nueva Carretera Aeropuerto Km 9.5, Apodaca, 66629, N.L., México; vcoello@cicese.mx

***Corresponding Author**
Jiří Homola
homola@ufe.cz
Institute of Photonics and Electronics
Chaberská 57, Prague, Czech Republic

## Abstract

The combination of microarray technologies with microfluidic sample delivery and real-time detection methods has the capability to simultaneously monitor 10s to 1000s of biomolecular interactions in a single experiment. Despite the benefits that microfluidic systems provide, they typically operate in the laminar flow regime under mass transfer limitations, where large analyte depletion layers act as a resistance to analyte capture. By locally stirring the fluid and delivering fresh analyte to the capture spot, the use of passive mixing structures in a microarray environment can reduce the negative effects of these depletion layers and enhance the sensor performance. Despite their large potential, little attention has been given to the integration of these mixing structures in microarray sensing environments. In this study, we use passive mixing structures to enhance the mass transfer of analyte to a capture spot within a microfluidic flow cell. Using numerical methods, different structure shapes and heights were evaluated as means to increase local fluid velocities, and in turn, rates of mass transfer to a capture spot. These results were verified experimentally via the real-time detection of 20-mer ssDNA for an array of microspots. Both numerical and experimental results showed that a passive mixing structure situated directly over the capture spot can significantly enhance the binding rate of analyte to the sensing surface. Moreover, we show that these structures can be used to enhance mass transfer in experiments regarding an array of capture spots. The results of this study can be applied to any experimental system using microfluidic sample delivery methods for microarray detection techniques.

Keywords: microarrays, microfluidics, microfluidic mixing, mass transfer, biosensors.

## *1.* Introduction

A microarray is a two-dimensional set of specific biological capture probes deposited in an orderly grid of spots on a flat substrate, typically a glass slide. Each microarray spot contains one type of capture probe, and is immobilized to a region that is tens or hundreds of microns in diameter, herein referred to as a capture spot (Wu et al. 2012). Multiplexing capabilities are produced by spatially encoding the array, where each location serves as a reporter for a specific analyte (Situma et al. 2006). Microarrayers, the instruments used for the deposition of sample probes, typically operate with a positional resolution from 2.5 up to 5 μm, where the size of the spot can be varied through a selection of contact surface tips from around 30 to above 600 μm in diameter. To maximize the performance of the detection assays, it is important to increase the rate of mass transfer to the capture spot; an increase in the amount of captured analyte within a set assay time will lead to an assay with higher sensitivity. Microarray-based assays were initially carried out in a simple manner via the immersion of the microarray substrate into a target solution (Ekins and Chu 1991). The sensitivity of these static assays, measured as the diffusive analyte flux to the center of the capture spot, has shown to be inversely proportional to the capture spot diameter (Dandy et al. 2007; Ekins 1998). In this static regime the flux remains proportional to the analyte diffusivity, and mass transfer rates remain low for assays involving larger biomolecules having inherently low diffusivities.

Further increases in analyte mass transfer rates to a capture spot can be obtained through the addition of fluid convection to the system. The use of a shaking plate to stir fluid over a capture spot has been shown to provide dramatic increases in assay sensitivity (Kusnezow et al. 2006; Saviranta et al. 2004). To further exploit the use of convective fluid transport in the array sensors, many researchers have turned to the use of microfluidic continuous flow cells. These microfluidic flow cells provide several benefits to array technologies, including a reduction of reagent consumption, reduced footprints, and decreases in the characteristic time for diffusive mixing and surface reactions.

The use of microarray technologies in a microfluidic format has been used in multiple instruments that can simultaneously sense thousands of different samples per square centimeter in a flow chamber (Campbell and Kim 2007; Eddings et al. 2009; Homola et al. 2005; Piliarik et al. 2010; Piliarik and Homola 2008). The ability to simultaneously investigate large numbers of targets has been effectively applied in genomics (DNA microarrays) and proteomics (protein microarrays) on a regular basis. These experiments are useful in many areas, including the identification of biomarker catalogues for diagnosis and prognosis, to relate physiological states to gene or protein expression patterns, and to study the progression of diseases as well as cellular response to stimuli (Malic et al. 2011; Trevino et al. 2007).

Current microfluidic-based microarray technologies use simple rectangular microfluidic flow cells, where there is no change in the microchannel cross-section over the length of the array. However,

these benefits are also tied to the disadvantages of laminar flow, present due to the small characteristic lengths and fluid velocities encountered with microfluidics. For microarray systems under mass transfer limitations (where rates of analyte capture are much greater than the rate of analyte transport to the sensor), the lack of turbulence can lead to large analyte depletion layers that act as a resistance to analyte capture and detection. These depletion layers can also affect other similar capture spots situated directly downstream, which are subjected to lower concentrations of analyte. Several authors have taken steps to mitigate the effects of these depletion layers with the use of more complex pumping techniques. Adey *et al*. used an air bladder to pump fluid back and forth across a microarray chamber to improve hybridization rates (Adey et al. 2002). Furthermore, several authors have used alternating pairs of syringe pumps to periodically alter the flow direction within a microfluidic chamber, where the resulting flow profile serves to improve the performance of the microarray assay (Hertzsch et al. 2007; McQuain et al. 2004; Raynal et al. 2007). It should be noted, however, that although periodic changes in the microfluidic flow direction can serve to enhance the microarray performance, they do not modify the flow field to mitigate the presence of any analyte depletion layers. In this area there remains an opportunity for sensor improvement from the implementation of microfabrication techniques to modify the fluid flow profile only in the vicinity of each spot, while still allowing for the use of a simple, single source fluid delivery technique. Specifically, the use of passive mixing structures above each spot can serve to increase local rates of mass-transfer to each spot, thereby increasing the sensitivity of the assay.

Over the past 15 years there has been a large effort focused on enhancing the rate of mixing in microfluidic systems. These efforts can be divided into two broad categories, mixing via an active or passive manner. Active systems manipulate and mix fluid quickly (often in an adjustable manner) through a variety of mechanisms, including piezoelectric, thermal, acoustic, and magnetic methods (Hessel et al. 2005). Although these systems possess the ability to provide efficient mixing profiles, they are generally very complex and require additional equipment or materials. Furthermore, they often suffer from problems associated with heat transfer and bubble formation. In contrast, passive mixers have the ability to enhance fluid mixing without the requirement of supplementary energy while often employing a much simpler fabrication process (Beebe et al. 2002; Wu et al. 2004).

Despite the large amount of literature devoted to passive mixing techniques, there remains little information concerning the use of these mixers for the enhancement of mass transfer to a sensor surface. Liu *et al*. used a chaotic micromixer to mix the target solution (and remove depletion layers) entering and leaving a hybridization chamber (Liu et al. 2006); however, the mixer was situated outside the boundaries of the microarray, and the system required a built in peristaltic pump for operation. Several authors have utilized microfluidic mixers situated directly over the sensing chamber. Kirtland and Stroock used theoretical and numerical methods to show the benefits that chaotic mixing in a rectangular channel can have on mass transfer to a channel surface (Kirtland et al.

2006). In another numerical study, Forbes and Kralj examined optimal geometric designs of the staggered herringbone mixer for the enhancement of interaction between fluid streamlines and a sensing surface (Forbes and Kralj 2012). Experimentally, Golden *et al*. demonstrated an enhancement of binding for an affinity assay in a microchannel fabricated with grooved passive mixing structures (Golden et al. 2007). Similarly, Foley et al. showed only modest improvements in mass-transfer using similar structures (Foley et al. 2008). These studies utilized sensing domains consisting of a long reactive boundary of length 1-100 mm for the capture of a single analyte. Obviously, this characteristic size is much larger than that of a typical microarray, where within the same space using a microarray there might be hundreds or thousands of reactive surfaces, each having specificity for a unique analyte. To our knowledge there exists no information on the use of passive mixing structures to enhance the mass transfer of an analyte to a reactive surface having a characteristic size similar to a traditional microarray capture spot. The use of such structures has great potential in the enhancement of these microarrays; increases in mass transfer will lead to shorter assay times, and furthermore, a reduction in the microarray limit of detection.

In this paper we explore the utilization of passive mixing structures to increase the efficiency of mass transfer of analyte to an individual capture spot. Figure 1 shows the particular approach of this work, where passive mixing structures situated on the surface opposite of a capture spot serves to provide higher fluid velocities, and in turn, higher rates of analyte delivery. These benefits come at the expense of small increases in the viscous resistance of the channel; however, the additional pressure drops are negligible with respect to those that would be encountered by simply reducing the overall height of the channel. Furthermore, these structures act to stir the fluid for the prevention of any detrimental downstream effects, which would not be seen in a simple channel of reduced height.

Using computational methods, we examine how the shape of a several passive mixing structures affect local rates of mass transfer to a capture spot. Additionally, we examine the relationship between the positions of the passive mixing structures relative to the positions of the reactive spots on the sensor performance. The numerical results are verified experimentally using a self-referencing surface plasmon resonance (SPR) imaging sensor for the real-time detection of 20-mer single stranded DNA (ssDNA). We show that the passive mixing structures increase the binding rate of an analyte to a microarray spot with respect to a reference channel having no structures, both for a single spot as well as multispot arrays.

The results of this study can be applied to any study using microarray technologies with microfluidic analyte delivery techniques, including DNA biochips relying on fluorescent labeling (Stoughton 2005) or biosensors based on surface plasmon resonance imaging (SPRi) (Piliarik et al. 2010). In addition to microarray technologies, this methodology can be extended to other systems requiring the delivery of target solute to a localized area present on the surface of a microchannel (e.g. electrochemical detector).

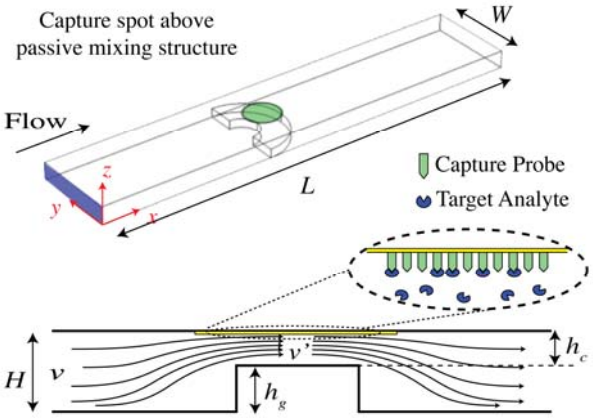


**Figure 1**. Example of the work presented here: a single passive mixing structure situated beneath a capture spot serves to increase the average fluid velocity near the spot (from $v$ to $v$') and increase local rates of mass transfer.

## 2. Methods

*Computational Simulations.* The passive structures used in this study can be characterized by having a height $h_g$, with a gap in between the structure and the top surface having a height $h_c$ (Fig. 1). In this configuration the upstream and downstream portions of the channel have a height $H=h_g+h_c$. The structures are located in a microchannel with width $W$, where a fluid with average velocity $v$ (measured in the upstream portion of the channel) carries an analyte with concentration $c$ and diffusivity $D$ towards the capture spot.

The capture of an analyte by a microarray spot is a complex process, involving the time-dependent microscopic convection and diffusion of analyte throughout the microfluidic flow cell. The analysis of this process can be simplified with a few well-justified assumptions. We first assume the binding of target analyte to capture probe follows an affinity relationship, where the analyte in the bulk solution reversibly binds to an immobilized capture probe. A good model system for this interaction is seen via the hybridization of 20-mer DNA. For this model system, the forward and reverse reaction rate constants and the concentration of surface probes can be assumed to be $k_1 = 2\times10^7$ $M^{-1}$ $s^{-1}$, $k_2 = 10^{-5}$ $s^{-1}$, and $b_o = 5\times10^{-14}$ mol $mm^{-2}$, respectively (Lynn et al. 2013; Sipova et al. 2012). These values are also typical for other nucleic acid, antibody/antigen, and aptamer microarrays. The operation regime of heterogeneous affinity assays operated under convective means are best described by the ratio of reactive to diffusive analyte flux to the capture spot, also known as the Damköhler number (Da),

$$\mathrm{Da} = k_1 b_o \delta / D \ , \qquad (1)$$

where $\delta$ is the thickness of the analyte depletion layer above the capture spot. If Da>>1, then the reactive flux is much larger than the diffusive flux, and the system becomes mass transport limited. Conversely, if Da<<1, the system is reaction limited. The depletion layer thickness is a function of the

Peclet number $\mathrm{Pe} = h_c v / D$, where an estimate of $\delta$ can be calculated as $\delta \approx \left( h_c^2 L / 6\mathrm{Pe} \right)^{\frac{1}{3}}$ (Squires et al. 2008). For a system with $h_c$ = 40 μm, $v$ = 0.15 mm $s^{-1}$, $L$ = 200 μm, and $D$ = $10^{-4}$ $mm^2$ $s^{-1}$, the Damköhler number can be calculated as Da = 96, and therefore it is safe to assume that the assay falls within the mass transfer limited regime in the early stages of the assay. Furthermore, for sufficiently low analyte concentrations, where $c << K_d$, we can assume that the sensor will not reach equilibrium in a reasonable time.

With these assumptions, the distribution of analyte within the fluidic chamber will resemble the steady-state solution to the convection-diffusion equation, where the analyte concentration on each capture spot is set to zero. A good metric for the performance of each structure can then be calculated as the diffusive flux ($J$) of analyte normal to its respective capture spot.

The evaluation of the performance of each structure is carried out numerically via the solution to the Navier-Stokes equations coupled to the convection-diffusion equation. The solutions to these equations were obtained using the COMSOL finite element package (ver. 4.2a), using linear and quadratic shape functions for the momentum and mass transport equations, respectively. The computational domains extended from a distance $W$ and 0.5$W$ upstream and downstream of each structure (or capture spots), respectively. The boundary conditions consisted of a fully developed fluid velocity profile at the inlet with average fluid velocity $v$, a zero pressure condition on the outlet, and a condition of $c$ = 0 on all capture spots. Using these boundary conditions, the solution for the velocity, pressure, and analyte concentrations were obtained using the Generalized Minimal Residual iterative solver, with a PARADISO course solver, using a successive over-relaxation method for the pre- and post-smoother. After convergence of the solutions, the normal diffusive flux of analyte toward each reactive spot was calculated using built in COMSOL functions. The solution to the convection-diffusion equation is prone to numerical errors for flows having a high mass transfer Peclet number (Finlayson 1980); therefore, it is necessary to find an appropriate mesh density such that all solutions converge to a state that is free from numerical error. We examined the diffusive flux towards the sensor surface as a function of the characteristic size of the mesh for simulations with constant Pe = 150 ($h_c$ = 10 μm, $H$ = 40 μm, $v$ = 150 μm/s, $D$ = $10^{-11}$ $m^2/s$), where the mesh was composed of triangular elements in the $x$,$y$-plane that were swept in the $z$-direction to form a hexahedral element. A mesh with a characteristic size of 1.5 μm ($x$,$y$-direction) and 0.5 μm ($z$-direction) was found to provide solutions that were independent of the mesh density. This meshing scheme corresponds to a total number of 3-5 million degrees of freedom, varying for each microstructure array.

*SPR imaging system and microfluidic flow cell.* A self-referencing SPR imaging sensor (Fig. 2) with polarization contrast was developed at the Institute of Photonics and Electronics in Prague, Czech Republic (Piliarik et al. 2010). This sensor is based on the Kretschmann geometry of the attenuated total reflection method and prism coupling of light into a surface plasmon (Raether 1988). In this

configuration, both the spatial distribution of intensity and polarization changes of the reflected light are measured and correlated with the spatial distribution of refractive index changes on the sensor surface. Specifically, a narrowband light emitted by a superluminescent diode (750 nm) is collimated and passed through a polarizer and made incident on the base of a coupling prism. An SPR chip (produced by evaporation of a 1 nm titanium adhesion layer followed by a 49 nm gold film onto a BK7 glass substrate) is attached directly to the prism surface via a refractive index matching fluid. Light reflected from the gold layer on the SPR chip (sensor surface) passes through the coupling prism, to a quarter-wave plate, and through another polarizer. A telecentric lens (Edmund optics GmbH, Germany) is used to image the sensor surface on a tilted CCD camera (sca780-54fm, Basler AG, Germany). A reference mirror is prepared on the prism surface, where the light reflected to the CCD camera provides a reference signal and enables for the real time compensation for fluctuations of intensity of incident light.

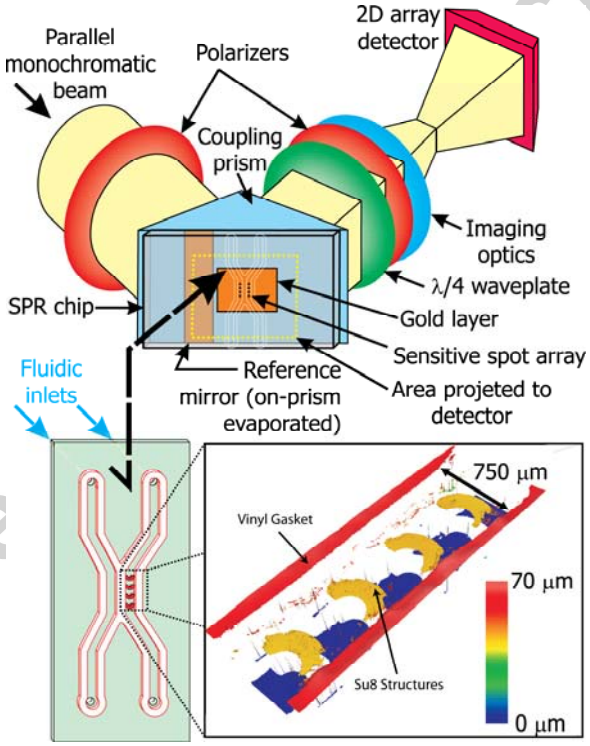


**Figure 2**. Diagram of the experimental imaging SPR setup used here. The fluidic cell consists of a vinyl gasket serving as the channel sidewalls (H = 65 μm), with passive mixing structures constructed of Su8 ($h_g$ = 40 μm). An optical profilometer scan of the channel having the mixing structures is seen on the lower right.

The microfluidic flow cell consists of a CR39 substrate (Edmund optics GmbH, Germany) with drilled fluidic inlets and outlets, onto which the semiloop structures were lithographically prepared using the Su8-based photoresist GM1070 (Gersteltec Engineering Solutions, Switzerland). The flow cell sidewalls were prepared from a gasket carved from a one-side soft vinyl sheet MACal® 9800 PRO (MACtac Prague, Czech Republic). After alignment to the semiloop structures, the vinyl gasket

acts to seal the flow cell when pressed against the SPR chip. The vinyl gasket was cut as to create a fluidic channel with a width of 750 μm, where the thickness of the gasket (after compression) was measured to be 65 ± 2 μm. In addition, the height of the semiloop structured was measured to be 40.0 ± 0.5 μm. The height and width of the fluidic channel was measured via an optical profilometer. A scan of the channel region containing the semiloop structures can be seen in Fig. 2.

*Sensing array and experimental conditions.* The SPR chips were first washed with ethanol and deionized water (DI), dried with nitrogen, and placed in a UV ozone cleaner for 10 min to remove any organic contaminants. After cleaning, the chip was again washed with ethanol and DI, and dried with nitrogen. An array of 300 μm diameter ssDNA microspots were prepared on the chip using a 10 μM solution of thiolated DNA probes (5'-5/ThioMC6-D/TAT TAA CTT TAC TCC CTT CC-3') in PBS buffer (10 mM phosphate, 2.9 mM KCL, 137 mM NaCl, pH 7.4) using a commercial Omnigrid microarrayer (Genomic Solutions) in an 85% humidity chamber. The array was left to incubate in the chamber for an additional 30 min before being mounted into the SPR imaging sensor. PBS was first injected into the sensing chamber at a volumetric flow rate of 20 μL/min for 15 minutes, after which the complementary DNA target (5'-GGA AGG GAG TAA AGT TAA TA-3') at a concentration of 100 nM in PBS was injected at the same flow rate for 20 minutes.

## 3. Results and Discussion

In this study we consider the sensing enhancement through the use of passive mixing structures fabricated on the surface opposite that of a capture spot. It is important to know how the shape of a passive mixing structure influences the rate of mass transfer to a capture spot (measured by the diffusive analyte flux *J*), how that rate of mass transfer compares to a reference channel of height *H*, and furthermore, the maximum level of mass transfer enhancement obtainable by each structure. For all sensors, an increase in *J* will result in an increase in the overall sensor performance and will lead, in particular, to higher sensor sensitivities as well as lower limits of detection (Dandy et al. 2007; Lynn et al. 2013; Sheehan and Whitman 2005; Squires et al. 2008).

When comparing passive mixing structures of different shape, it is important to keep the ratio $\varphi$ of the passive mixing structure height to the overall height of the channel constant, where $\varphi = h_g / H$. This is due to the large effect of the average fluid velocity in the vicinity of the reactive spot on the analyte flux (Squires et al. 2008). The steady-state diffusive flux of analyte to a sensor surface of length *L* occupying the entire width of the channel can be described as

$$J \approx c\left(\frac{6D^2 v}{LH}\right)^{\frac{1}{3}}, \qquad (2)$$

which was derived in a previous study using the same assumptions described above (Lynn et al. 2013). Fluid passing through the constriction between the passive mixing structure and the sensor

surface will have an increased velocity on the order of $v' = v/(1-\varphi)$; however, the distribution of this increased velocity field (and thus the distribution of increased $J$) will vary according to the overall shape of each structure.

Figure 3A displays three passive mixing designs that are considered in this study: a herringbone groove, a slanted groove, and a semiloop. Periodic arrays of the herringbone and slanted groove structures have been previously studied for the enhancement of sensors (Golden et al. 2007; Kirtland et al. 2006) whereas the effect of the semiloop structure has been unexplored. We first examine the mass transfer enhancement of each structure within a common environment, where each structure was centered in a sensing domain with an area of $W^2$, as shown in Fig. 3A. This situation is representative of the use of microfluidic channels for the immobilization of capture bodies to a sensor surface (Bernard et al. 2001).

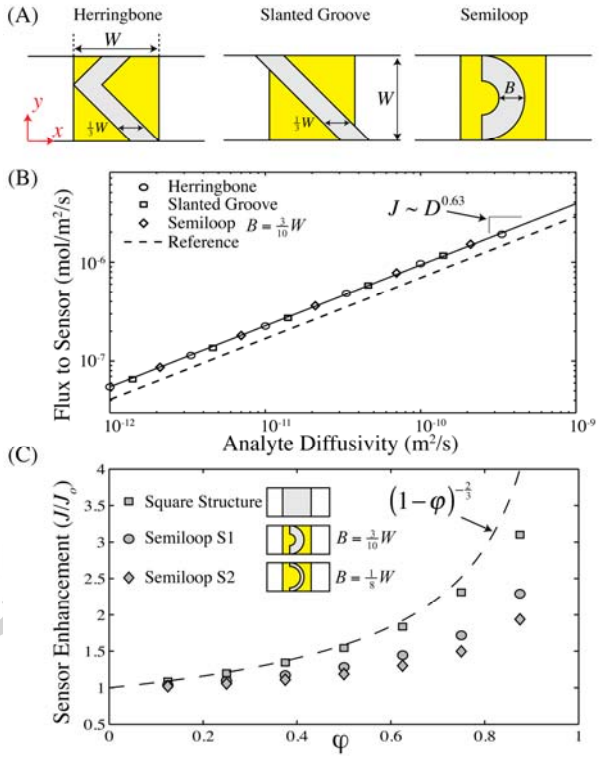


**Figure 3**. (A) Overall shape of the herringbone, slanted groove, and semiloop structures, the yellow regions indicate the sensing surface on the opposite side of the channel. (B) Analyte flux to the sensor surface as a function of the analyte diffusivity for a channel with $\varphi = 0.5$. The solid line represents a power law fit through the data for all 3 structures, the dashed line is the response of a reference sensor of height $H$ = 40 μm. (C) Sensor enhancement $J/J_o$ vs. the groove height ratio $\varphi$ for three structures, semiloop S1, semiloop S2, and a block structure having the same area and position as the sensor surface.

Figure 3B plots the analyte flux to the sensor surface for the three structures as a function of the analyte diffusivity for a sensor with $H$ = 40 μm, $\varphi = 0.5$, $W$ = 200 μm, $c$ = 0.1 nM, and $v$ = 0.15 mm/s. It can be seen that $J$ increases with increasing $D$, where the relationship follows the trend $J \sim D^{-0.63}$ for all three structures. This behavior is similar to the trend of $J \sim D^{\frac{2}{3}}$, predicted via Eqn. 2. The

analyte flux $J_o$ to a reference sensor situated in a channel of height $H$ (having no passive mixing structures) is shown in the dashed line. The level of sensing enhancement due to the passive mixing structures can thus be estimated by the ratio between $J$ and $J_o$ at a constant diffusivity. For example, at low analyte concentrations, a sensor using passive mixing structures having an enhancement ratio of $J/J_o$ = 1.6 will bind 60% more material than a reference sensor in the same assay time period. All of the structures shown in Fig 3B have a sensing enhancement of $J/J_o \approx 1.30$, regardless of the diffusivity. Despite the large differences in the fluid velocity fields surrounding these three structures, values of $J$ for the three structures simulated at similar diffusivities varied by less than 1% from one another. This is most likely due to the similarities in surface area (in the $x$,$y$-plane) between the three structures, where the semiloop structure has a surface area ($0.330W^2$) that is only 1% less than the surface areas of the herringbone and slanted groove structures ($0.333W^2$) compared with the semiloop structure.

From Eqn. 2, it is expected that the groove height ratio will have the most effect on the level of diffusive flux enhancement. Figure 3C displays $J/J_o$ vs. $\varphi$ for two semiloop structures with $B = \frac{3}{10}W$ and $B = \frac{1}{8}W$, noted here as S1 and S2, as well as a square structure of area $W^2$. The square structure is for comparison, and is situated directly over the sensing area. As expected, there is an increase in $J/J_o$ with increasing $\varphi$ for all structures. These data scale roughly as $J/J_o \sim (1-\varphi)^{\alpha}$, where $\alpha$ has values of -0.55, -0.41, and -0.32 for the block, S1, and S2 structures, respectively. The upper limit of sensing enhancement for a single structure can be estimated as the case where the sensing surface lies completely beneath the structure itself, having a new sensor height of $h_c = H(1-\varphi)$ and an average fluid velocity of $v' = v/(1-\varphi)$. From Eqn. 2, this optimal sensing enhancement can then be calculated as

$$J_{opt}/J_o = (1-\varphi)^{-\frac{2}{3}}. \quad \textbf{(3)}$$

Equation 3 is plotted as the dashed line in Fig. 3C. It should be noted that for low analyte concentrations this enhancement is independent of many parameters important to a biosensing process (i.e. volumetric flow rate, channel width and height). It can be seen that the sensing enhancement for the three structures (constant $\varphi$) approaches the optimum level as the size (or surface area) of each structure increases. The differences between $J/J_o$ from the square structures and the optimal levels predicted via Eqn. 3 can be attributed to the converging and diverging flows in the upstream and downstream portions of each structure, respectively, as well as in the assumptions used to derive Eqn. 2. Because of their lower footprint size, the sensor enhancement from the semiloop structures is much lower than the block structures, where for $\varphi$ = 0.5 the enhancement is 1.28 and 1.19 for the S1 and S2 structures, respectively.

The results in Fig. 3 show that the footprint size of a passive mixing structure has a strong influence on the enhancement of diffusivity flux to a sensor surface. Optimal behavior will be observed when the footprint size of a mixing structure approaches the surface area of an active sensor, or simply, when the capture spot lies directly within the gap between the mixing structure and the opposite surface. Because the semiloop structures in Fig. 3C are much smaller in size with respect to the sensing area (in the $x$,$y$-plane), the level of diffusive flux enhancement is much smaller than the optimal value predicted via Eqn. 3. In this case, the enhancement becomes more or less independent of the structure position as long as the structure fits entirely within the $x$,$y$-area of the active surface. Conversely, when the size of the active sensing area is reduced (as the case of a traditional microarray capture spot), the relative position between the capture spot and structure gains importance.

Due to their symmetric shape, the semiloop structures were chosen for the study of the effect of the spot position on the diffusive flux enhancement. The spot position with respect to the passive mixing structure can be defined by the axial distance from the start of the structure to the center of a circular capture spot ($d_x$) as well as the distance between the spot center and the centerline of the channel ($d_y$). Figure 4 displays $J/J_o$ vs. the axial spot position along the channel centerline ($d_y = 0$) for both the S1 and S2 semiloop structures in a channel with $H$ = 40 μm, $W$ = 200 μm, $v$ = 0.15 mm/s, and a spot diameter $d_s = \frac{3}{10}W$. The dashed lines represent the optimum enhancements predicted via Eqn. 3. It can be seen that the enhancement values for the larger S1 structure are always higher than the respective values for the smaller S2 semiloop structure (constant $\varphi$, $d_x$), where the maximum enhancement level of the S1 structure approaches that of the maximum level predicted via Eqn. 3 at all groove height ratios.

Interestingly, the maximum enhancement for the S1 semiloop occurs at a position such that there is a significant portion of the capture spot lying outside the footprint of the semiloop structure, where $d_x = 0.25W$. This effect is also seen in the results of structure S1, and is a result of the converging flow field just upstream of the structure. To understand how the $y$-direction of the spot position influences the sensor enhancement, we obtained solutions for the diffusive flux to a capture spot for a 9×5 array of spot positions (equally spaced in the $x$- and $y$-directions). The simulations were performed on one side of the symmetry plane, in the domain of $0 < d_y < 0.5W$ and $0 < d_x < W$. The results of this array sweep, for both the S1 and S2 structures, are shown in the contour plots in Fig. 4. It should be noted that the diffusive flux to a reference channel of height $H$ is independent of the spot position. Both structures have a small dependence on $d_y$ with respect to $d_x$. As expected, the areas of maximum enhancement lie where the spot is situated either directly underneath or directly upstream of the passive mixing structure.

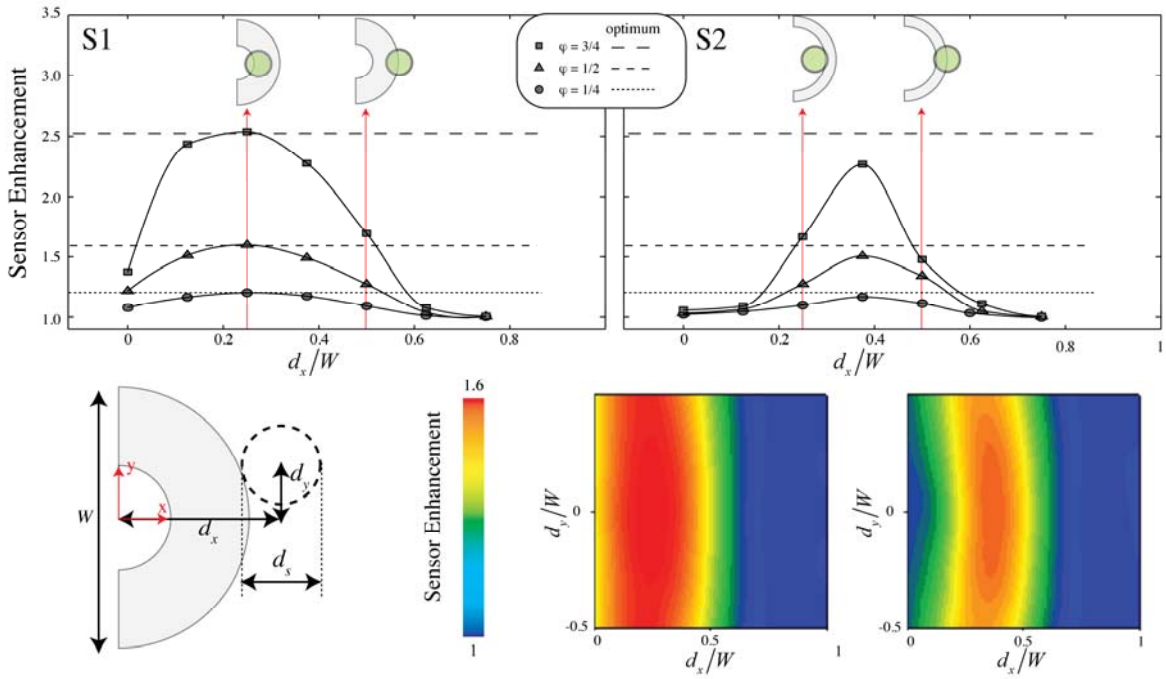


**Figure 4**. (Bottom left) A capture spot with diameter $d_s$ lies at an axial distance $d_x$ from the start of a structure, with a distance $d_y$ away from the centerline. (Top) Sensor enhancement ($J/J_o$) vs. dx along the centerline ($d_y = 0$) for the semiloop structures S1 and S2. (Bottom right) contour plot of the sensor enhancement vs. the *x*- and *y*-position of the capture spot ($d_s$ = 60 μm, $W$ = 200 μm, $H$ = 40 μm, $\varphi$ = 0.5).

The results shown in Figures 3 and 4 can be used to draw several guidelines regarding the design of these structures for sensing enhancement purposes. Although periodic arrays of these structures may be used for mixing purposes, a single structure only serves to stir the fluid, and there is negligible convective fluid mixing occurring on the length scale of the active sensing surface. As a result, the mechanisms for the enhancement of diffusive analyte flux to the sensor proceed through (*i*) an increase in the local fluid velocity around the sensing spot, and (*ii*) a reduction in the channel height in the vicinity of each spot. The combination of these two factors leads to Eqn. 3, which is solely a function of the groove height ratio $\varphi$, and can be used to calculate the maximum level of expected sensing enhancement (the maximum level of analyte flux increase).

This sensing enhancement comes at the expense of an increased pressure drop through the system. To estimate the level of increased pressure drop from a single structure, it is useful to examine the system via an analogous viscous resistance network. The pressure drop $\Delta p$ through a microchannel (assuming laminar flow) can be calculated via $\Delta p = -QKL_{ax}$, where $Q$ is the volumetric flow rate through the channel, $L_{ax}$ is the axial length of the channel, and $K$ is the viscous resistance to flow. Neglecting secondary effects due to sudden contractions and expansions from the passive mixing structures, $K$ can be calculated as

$$K = \frac{12\mu}{W^3 H}\left[1 - \frac{192W}{\pi^5 H}\sum_{n=1,3,5\ldots}^{\infty}\frac{1}{n^5}\tanh\left(\frac{n\pi H}{2W}\right)\right]^{-1}, \qquad \textbf{(4)}$$

where $\mu$ is the viscosity of the fluid (Rohsenow and Hartnett 1973). For channel aspect ratios near $H/W \approx 1$, the viscous resistance of the channel will scale as $K \sim H^{-2}$. Conversely, for a channel aspect ratio of $H/W << 1$, the dependence on the channel height increases, and $K$ will scale as $K \sim H^{-3}$. It follows that the viscous resistance caused by the structure will scale as $K_s \sim (1-\delta)^{-\beta}$, where $\beta$ is dependent on the channel aspect ratio and is in the range of $2 < \beta < 3$.

For systems where the volumetric flow rate is constant, such as flows generated by a peristaltic or syringe pump, one can calculate the pressure drop via the sum of $QK_rL_{ax,r}$ and $QK_sL_{ax,s}^{'}$, the viscous resistance of the channel upstream (and downstream) of the structure and the resistance due to the structure, respectively. Because of the linear relationship between $\Delta p$ and $L_{ax}$, the increased pressure drop due to the presence of a mixing structure will be much lower with respect to the case of reducing the entire channel height from $H$ to $h_c$. For example, we examine the pressure drop increases due to a semiloop structure ($L_{ax,s} = 0.5W$) in a channel with $H$ = 40 μm, $W$ = 200 μm, and 0.5 mm of clearance upstream and downstream of the structure. For the semiloop structure, the increase in pressure drop relative to a reference channel $\Delta p/\Delta p_o$ will be 1.1, 1.6, and 6.5 for structures having a height ratio of $\varphi$ = 0.25, 0.5, and 0.75, respectively. By reducing the channel height to $h_c$, these respective increases in pressure drop change to 2.4, 8, and 62. Essentially, the passive mixing structures provide the benefits of a smaller channel at the expense of a relatively small increase in the pressure drop compared to a channel with a smaller height.

The design of these structures for the enhancement of a single capture spot is fairly straightforward; a structure having a footprint that bounds the $x$,$y$-area of the capture spot will provide for an optimized system in terms of sensing enhancement. For the enhancement of multiple spots situated in a periodic arrangement with a pitch $\Lambda$, the situation is somewhat more complicated. To avoid potential depletion layer effects on downstream capture spots (having the same analyte specificity), the structure needs to be designed such that the fluid is stirred and fluid streamlines are perturbed to deliver fresh analyte to the downstream spot. Although a simple block structure works well for a single spot, it provides no transverse component to the velocity field and will not be adequate for a multi-spot assay. In contrast, the semiloop provides a bi-helical flow profile similar to that of a symmetric herringbone groove and is expected to aid in the replenishment of the depletion layer (for the enhancement of downstream spots). Numerical predictions of the sensing enhancement these arrays provide are difficult to obtain, as there are unavoidable errors associated with numerical diffusion for the swirling flows, even at moderate Péclet numbers. The use of particle tracking techniques can provide an accurate model of these systems (Kirtland et al. 2006); however, the analysis of the dimensionless characteristics of mixing with a heterogeneous reaction is complex and outside the scope of this study. In that case, we

turn to experimental methods for a proof of concept test of the use of these structures for sensing enhancement.

The experiments performed here serve both as verification for the numerical experiments detailed in Fig. 3 and 4 as well as an exploratory look into how the semiloop structures aid in multi-spot simulations. We utilized an SPR imaging sensor for the analysis of 20-mer ssDNA binding to a sensing spot of diameter $d_s$ = 300 μm in a channel with $W$ = 750 μm and $H$ = 65 μm. The microfluidic flow cell had two channels: one reference channel with no structures, and one channel with the S1 semiloop structures of height $h_g$ = 40 μm situated at a pitch of $\Lambda$ = 750 μm in a position of $d_x = 0.25W$ and $d_y$ = 0. An image produced by an optical profilometer of the mixing channel is seen in Fig. 2. The spots were printed to an SPR chip with the same pitch as the structures, after which the chip was aligned to the semiloop structures using a set of alignment pins and mounted to the SPR imaging sensor. After injection of the target ssDNA into the flow chamber ($Q$ = 20 μL/min, $v$ = 6.8 mm/s), we recorded the signal intensity as a function of time reflected from the 4 spots in both the reference and signal channels. In the SPR imaging instrument, the signal intensity is proportional to the local refractive index change in the region just above the sensor surface, which in turn is proportional to the amount of specifically bound target analyte on the sensor surface. Therefore, an increase in signal implies an increase in the amount of bound material on the sensor, and moreover, the 1$^{st}$ derivative of that time-series signal (the binding rate) is proportional to the diffusive analyte flux of target analyte to each capture spot.

Figure 5A shows the sensor response vs. time regarding the binding of 20-mer ssDNA to spot 1 and spot 4 in both the reference and mixing channel. The sensor response increases at a higher rate for the semiloop structures compared to the respective spots in the reference channel. By taking the 1$^{st}$ derivative of this data (using a 4$^{th}$ order finite difference scheme), the binding rate for each spot can be obtained. Figure 5B shows the binding rate vs. time for the 20-mer ssDNA to the 4 microarray spots in both the reference and mixing channel. It can be seen that upon target analyte injection, the binding rate increases for each spot to a maximum value ($t$ = 2 min), after which the binding rate slowly decays to zero as equilibrium effects start to take place (due to the higher, 100 nM analyte concentration). For both the reference and mixing channels, the maximum binding rate is the highest for the 1$^{st}$ spot and decreases with increasing spot number. Furthermore, the binding rate in the semiloop channels is higher than that in the reference channels, where the maximum binding rates decrease at a slower pace with increasing spot number (with respect to the reference channel). The level of sensing enhancement in the experimental system can be calculated as the ratio of the maximum binding rates between the mixing and reference channels. The results shown in Fig. 5B were repeated for 6 individual SPR chips, and the levels of enhancement for the combined experiments are shown in Fig. 5C. The mean sensing enhancement for the 6 experiments was 1.09, 1.18, 1.24, and 1.31.

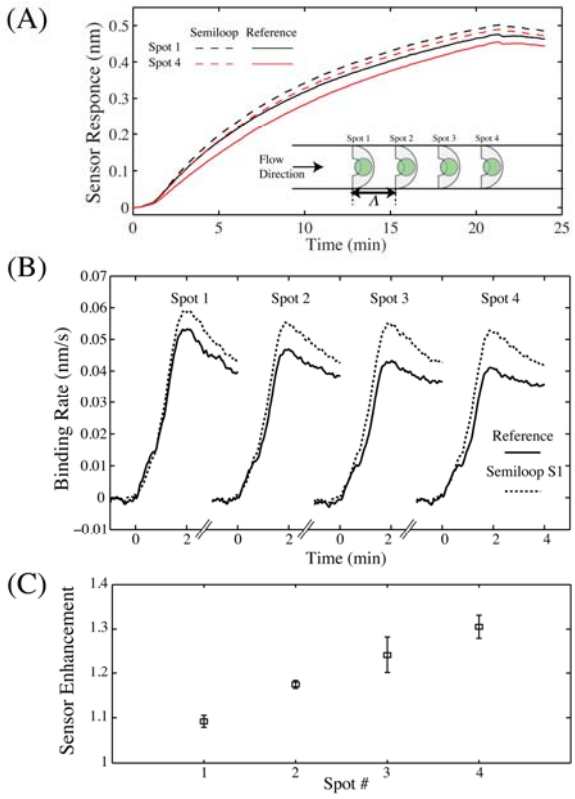


**Figure 5**. (A) The temporal sensor response to the binding of 20-mer ssDNA to spot 1 and spot 4 in both the reference and mixing channels. (B) The binding rate of 20-mer ssDNA as a function of time to the four capture spots in the reference channels as well as the channels having the S1 semiloop structures. (C) Sensor enhancement for the four spots (6 experiments).

The groove ratio for the experimental system shown in Fig. 5 was $\varphi = 0.62$, which via Eqn. 3 gives an optimal sensing enhancement of 1.90. The differences between this optimal value and the experimental values (for spot 1) can be attributed to several factors, including non-optimal fabrication and alignment of the S1 structures. The experiment was designed to print the spots with a ($d_x$, $d_y$) position of (0.25$W$, 0). Unfortunately, after the alignment of the printed SPR chip to the microfluidic flow cell, there is no way to measure the relative positions between the spots and structures. Although the 4 spots were well within the channel for all of the experiments conducted here (confirmed via SPR imaging), the current methods of chip alignment have a precision of ± 200μm, and the $x$-position of the spots was likely sub-optimal. Another issue is with the alignment of the vinyl gaskets to the semiloop structures, where in the current setup there was a small gap between the vinyl gasket (channel sidewalls) and the S1 structures. This creates an alternative path for fluid travel, resulting in lower fluid velocities in the region near the spot, thus lower values of $J$. Fabrication methods providing higher precision alignment between the printed SPR chip and the microchannel structures is the focus of future work, where channels are fabricated from multiple layers of Su8 (rather than the current vinyl/Su8 approach). Despite this sub-optimal capture spot placement, it is clear that the structures have a positive effect on removing the depletion layer for downstream spots, as the mean sensing

enhancement for the 6 experiments increased from 1.09 for spot 1 to 1.31 for spot 4. From the results of Kirtland and Strook (Kirtland et al. 2006), it is expected that the shape of the passive mixing structures play a significant role in the relationship between the sensing enhancement and the spot number (where the flow field over multiple mixing structures should mix the fluid via Lagrangian chaos). This topic, as well as the upper limit of the sensing enhancement for a large array of capture spots, is the focus of future research.

The effect of the sensor enhancement seen both in the numerical (Figs. 3, 4) and experimental (Fig. 5) portions of this work are discussed as follows. The sensor enhancement discussed herein relates the ratio of the initial flux to the sensor surface using a passive mixing structure (which, as shown experimentally, is proportional to the binding rate) to the flux of a reference channel. For a given transduction mechanism with a constant footprint, in a sensor in the mass transfer limited regime ( Da>>1) having a higher analyte flux. more material will bind to the sensor surface in a given assay time. In this regime, the characteristic time $\tau$ for the sensor to achieve equilibrium can be expressed as $\tau \sim b_{eq}/J$ , the ratio of the surface density of capture sites at equilibrium to the analyte flux to the surface (Squires et al. 2008). Therefore sensors exhibiting a higher analyte flux will reach equilibrium in a shorter time period. Furthermore, for assays restricted to a time such that equilibrium is not reached, a sensor having a higher initial flux will obtain a higher degree of hybridization between analyte and capture probe. This effect can be seen experimentally in the results shown by Dandy et al. (Dandy et al. 2007).

In experimental systems, the number of free binding sites will decrease over time as hybridization progresses. From Eqn. 1, the system will then undergo a slow conversion from being mass transfer limited to one that is reaction limited. Therefore, the average flux to each capture spot will decrease as time increases. This effect, commonly seen in all time-series affinity assay binding curves, can also be seen in Fig. 5B: after $t$ = 2 min there is a slow decrease in the binding rate over time, where the binding rate is proportional to $J$. It is important to note here that if a sensor has an initial flux that is higher when compared to a reference, it will remain higher for the duration of the experiment. This can also be seen in Fig. 5, where the sensor response vs. time (Fig. 5A) as well as the binding rate vs. time (Fig. 5B) are higher for the passively mixed channels with respect to the reference channel for the duration of the experiment. Therefore, it is expected that the sensors having the passive mixing structures will exhibit a reduced limit of detection (LOD) with respect to a reference channel and that, the reduction of LOD will be inversely proportional to the sensor enhancement. An example of this behavior can be seen in our previous work, where an increase in the binding rate of a sensor (produced by reducing the sensing chamber height from $H$ = 47 μm to 7 μm) resulted in a decrease in the LOD from 20 pM to 5 pM (Lynn et al. 2013).

## 4. Conclusions

Here we have presented a method to enhance the sensing performance of microarray-based microfluidic assays using passive mixing structures. These mixing structures work by increasing the local fluid velocity in the region between the structure and the opposite surface. This increase in fluid velocity, combined with a decrease in the channel height *H*, leads to an increase in the diffusive analyte flux *J* to the microarray spot with respect to a reference channel with no structures. The use of these passive mixing structures will lead to a maximum sensor enhancement of $(1-\varphi)^{-\frac{2}{3}}$, where $\varphi$ is the ratio of the passive mixing structure height $h_g$ to the channel height. The level of enhancement is related to the relative surface areas (as well as the relative positions) between the microarray spot and the mixing structure, and comes at the expense of an increased pressure drop through the channel. In addition to enhancing a single spot, we have shown that these passive mixing structures lead to the enhancement to multiple microarray spots situated downstream from one another. The involvement of the shape of each structure for mixing purposes, as well as the optimum sensing enhancement these structures provide in large arrays of microspots, are the focus of future work. The results of this study can be applied to any study using microarray technologies using microfluidic analyte delivery techniques.

## 5. Acknowledgements

This research was supported by Praemium Academiae of the Academy of Sciences of the Czech Republic and the Czech Science Foundation (contract P205/12/G118). Coello-Cardenas acknowledges financial support from CONACyT Mexico, Project: CB-2009-01, 000000000127589. Additional support was provided by The Research Chair of Intelligent Machines at Tecnológico de Monterrey. The authors thank Ivo Tichy and Karel Chadt for their help in the experimental portions of the project.

## 6. References

Adey, N.B., Lei, M., Howard, M.T., Jensen, J.D., Mayo, D.A., Butel, D.L., Coffin, S.C., Moyer, T.C., Slade, D.E., Spute, M.K., Hancock, A.M., Eisenhoffer, G.T., Dalley, B.K., McNeely, M.R., 2002. Gains in sensitivity with a device that mixes microarray hybridization solution in a 25-mu m-thick chamber. Analytical Chemistry 74(24), 6413-6417.

Beebe, D.J., Mensing, G.A., Walker, G.M., 2002. Physics and applications of microfluidics in biology. Annu Rev Biomed Eng 4, 261-286.

Bernard, A., Michel, B., Delamarche, E., 2001. Micromosaic immunoassays. Analytical Chemistry 73(1), 8-12.

Campbell, C.T., Kim, G., 2007. SPR microscopy and its applications to high-throughput analyses of biomolecular binding events and their kinetics. Biomaterials 28(15), 2380-2392.

Dandy, D.S., Wu, P., Grainger, D.W., 2007. Array feature size influences nucleic acid surface capture in DNA microarrays. Proceedings of the National Academy of Sciences of the United States of America 104(20), 8223-8228.

Eddings, M.A., Eckman, J.W., Arana, C.A., Papalia, G.A., Connolly, J.E., Gale, B.K., Myszka, D.G., 2009. "Spot and hop": Internal referencing for surface plasmon resonance imaging using a three-dimensional microfluidic flow cell array. Anal Biochem 385(2), 309-313.

Ekins, R.P., 1998. Ligand assays: from electrophoresis to miniaturized microarrays. Clin Chem 44(9), 2015-2030.

Ekins, R.P., Chu, F.W., 1991. Multianalyte Microspot Immunoassay - Microanalytical Compact-Disk of the Future. Clin Chem 37(11), 1955-1967.

Finlayson, B.A., 1980. Nonlinear analysis in chemical engineering. McGraw-Hill International Book Co., New York ; London.

Foley, J.O., Mashadi-Hossein, A., Fu, E., Finlayson, B.A., Yager, P., 2008. Experimental and model investigation of the time-dependent 2-dimensional distribution of binding in a herringbone microchannel. Lab on a Chip 8(4), 557-564.

Forbes, T.P., Kralj, J.G., 2012. Engineering and analysis of surface interactions in a microfluidic herringbone micromixer. Lab on a Chip 12(15), 2634-2637.

Golden, J.P., Floyd-Smith, T.M., Mott, D.R., Ligler, F.S., 2007. Target delivery in a microfluidic immunosensor. Biosensors & Bioelectronics 22(11), 2763-2767.

Hertzsch, J.M., Sturman, R., Wiggins, S., 2007. DNA microarrays: Design principles for maximizing ergodic, chaotic mixing. Small 3(2), 202-218.

Hessel, V., Lowe, H., Schonfeld, F., 2005. Micromixers - a review on passive and active mixing principles. Chem Eng Sci 60(8-9), 2479-2501.

Homola, J., Vaisocherova, H., Dostalek, J., Piliarik, M., 2005. Multi-analyte surface plasmon resonance biosensing. Methods 37(1), 26-36.

Kirtland, J.D., McGraw, G.J., Stroock, A.D., 2006. Mass transfer to reactive boundaries from steady three-dimensional flows in microchannels. Physics of Fluids 18(7).

Kusnezow, W., Syagailo, Y.V., Ruffer, S., Baudenstiel, N., Gauer, C., Hoheisel, J.D., Wild, D., Goychuk, I., 2006. Optimal design of microarray immunoassays to compensate for kinetic limitations - Theory and experiment. Mol Cell Proteomics 5(9), 1681-1696.

Liu, J., Williams, B.A., Gwirtz, R.M., Wold, B.J., Quake, S., 2006. Enhanced signals and fast nucleic acid hybridization by microfluidic chaotic mixing. Angew Chem Int Edit 45(22), 3618-3623.

Lynn, N.S., Sipova, H., Adam, P., Homola, J., 2013. Enhancement of affinity-based biosensors: effect of sensing chamber geometry on sensitivity. Lab on a Chip 13(7), 1413-1421.

Malic, L., Veres, T., Tabrizian, M., 2011. Nanostructured digital microfluidics for enhanced surface plasmon resonance imaging. Biosensors & Bioelectronics 26(5), 2053-2059.

McQuain, M.K., Seale, K., Peek, J., Fisher, T.S., Levy, S., Stremler, M.A., Haselton, F.R., 2004. Chaotic mixer improves microarray hybridization. Anal Biochem 325(2), 215-226.

Piliarik, M., Bockova, M., Homola, J., 2010. Surface plasmon resonance biosensor for parallelized detection of protein biomarkers in diluted blood plasma. Biosensors & Bioelectronics 26(4), 1656-1661.

Piliarik, M., Homola, J., 2008. Self-referencing SPR imaging for most demanding high-throughput screening applications. Sensor Actuat B-Chem 134(2), 353-355.

Raether, H., 1988. Surface-Plasmons on Smooth and Rough Surfaces and on Gratings. Springer Tr Mod Phys 111, 1-133.

Raynal, F., Beuf, A., Plaza, F., Scott, J., Carriere, P., Cabrera, M., Cloarec, J.P., Souteyrand, E., 2007. Towards better DNA chip hybridization using chaotic advection. Physics of Fluids 19(1).

Rohsenow, W.M., Hartnett, J.P., 1973. Handbook of heat transfer. McGraw-Hill, New York,.

Saviranta, P., Okon, R., Brinker, A., Warashina, M., Eppinger, J., Geierstanger, B.H., 2004. Evaluating sandwich immunoassays in microarray format in terms of the ambient analyte regime. Clin Chem 50(10), 1907-1920.

Sheehan, P.E., Whitman, L.J., 2005. Detection limits for nanoscale biosensors. Nano Lett 5(4), 803-807.

Sipova, H., Vrba, D., Homola, J., 2012. Analytical Value of Detecting an Individual Molecular Binding Event: The Case of the Surface Plasmon Resonance Biosensor. Analytical Chemistry 84(1), 30-33.

Situma, C., Hashimoto, M., Soper, S.A., 2006. Merging microfluidics with microarray-based bioassays. Biomol Eng 23(5), 213-231.

Squires, T.M., Messinger, R.J., Manalis, S.R., 2008. Making it stick: convection, reaction and diffusion in surface-based biosensors. Nature Biotechnology 26(4), 417-426.

Stoughton, R.B., 2005. Applications of DNA microarrays in biology. Annu Rev Biochem 74, 53-82.

Trevino, V., Falciani, F., Barrera-Saldana, H.A., 2007. DNA microarrays: a powerful genomic tool for biomedical and clinical research. Mol Med 13(9-10), 527-541.

Wu, D., Song, L.B., Chen, K., Liu, F., 2012. Modelling and hydrostatic analysis of contact printing microarrays by quill pins. Int J Mech Sci 54(1), 206-212.

Wu, Z.G., Nguyen, N.T., Huang, X.Y., 2004. Nonlinear diffusive mixing in microchannels: theory and experiments. J Micromech Microeng 14(4), 604-611.